THE JOURNAL OF BIOLOGICAL CHEMISTRY
Vol. 270, No. 42, Issue of October 20, pp. 24693–24701, 1995
Printed in U.S.A.

Effect of pH on the Conformation and Backbone Dynamics of a 27-Residue Peptide in Trifluoroethanol

AN NMR AND CD STUDY*

(Received for publication, April 14, 1995, and in revised form, August 7, 1995)

Francis Fan and Kevin H. Mayo‡

From the Department of Biochemistry, Biomedical Engineering Center, University of Minnesota, Minneapolis, Minnesota 55455

The C-terminal fragment, residues 385–411, from human fibrinogen γ-chain, *i.e.* KIIPFNRLTIGEGQQHHLGGAKQAGDV, shows multiple turn conformations in aqueous solution (Mayo, K. H., Burke, C., Lindon, J. N., and Kloczewiak, M. (1990) *Biochemistry* 29, 3277–3286). The present study investigates the effect of pH and trifluoroethanol on the conformation and backbone dynamics of this 27-residue peptide. Both circular dichroism (CD) and ^{1}H-NMR data indicate the normally observed increased helical conformations as a function of increasing trifluoroethanol. ^{1}H-NMR structural studies done in the presence of 40% trifluoroethanol, pH 5.3, yield a network of nuclear Overhauser effects consistent with significant populations of helix-like conformation. Distance geometry calculations based on nuclear Overhauser effect-derived distance constraints yield a family of structures with relatively well defined N- and C-terminal conformations and an ill defined mid-peptide region from Gly^{397} to Gly^{403}. Similar conformational populations are observed at pH 2.5. CD studies, however, indicate an increase in average α-helix content on decreasing the pH from 6 to 2. This apparent conflict between CD and NMR results may be explained by a transition from multiple β-turn character at pH 5.3 to increased α-helix structure at pH 2.5. $^{13}C_\alpha$ NMR relaxation data analyzed with the Lipari-Szabo model-free approach provide order parameters that demonstrate little if any influence of pH on backbone motional restrictions within the more flexible mid-peptide domain. At low pH, however, motions become less restricted within N-terminal residues Lys^{385}–Phe^{389} and more restricted within C-terminal residues Ala^{405}–Val^{411}.

Protein folding is primarily dictated by noncovalent, relatively weak intramolecular forces, *i.e.* hydrogen bonding, electrostatic interactions, and hydrophobic effects (Jaenicke, 1991). The effect of pH and alcohols on protein structure and folding has been discussed widely in the literature. Depending on the protein, acids can generate either fully or partially denatured states (Kuwajima, 1992). For β-lactamase, apomyoglobin, and ferricytochrome *c* (Goto *et al.*, 1990), lowering the pH to about 2 by adding HCl yields unfolded proteins whose conformations can be partially stabilized into more compact states containing substantial secondary structure by the addition of more HCl. More complex pH-induced folding transitions have been observed at pH 2.7 with barnase (Sanz *et al.*, 1994). Alcohols have been known for some time both to denature/destabilize globular protein tertiary (Conio *et al.*, 1970; Parodi *et al.*, 1973) and quarternary (Yang *et al.*, 1993) structure and to effect conformational stabilization of various peptides in aqueous solution (Conio *et al.*, 1970; Parodi *et al.*, 1973). While some of these pH- and alcohol-induced states may be true protein folding intermediates, the presence of alternatively folded structures cannot be excluded. Nevertheless, their study can shed light on general principles of protein folding and dynamics.

Recently, more and more short linear peptides are being used as models for protein folding and local structure formation. Although this approach has been exemplified with synthetic peptides derived from the α-helix protein myoglobin (Waltho *et al.*, 1993; Shin *et al.*, 1993a, 1993b) and the mostly β-sheet protein platelet factor-4 (Ilyina *et al.*, 1994), studies on the ribonuclease S peptide (20 residues) (Brown and Klee, 1971) and pentapeptides like YPGDV (Dyson *et al.*, 1988a, 1988b) first fueled the fire of interest in others. NMR and CD, in particular, have been used to show that short linear peptides can have considerable conformational populations in aqueous solution in the presence and absence of various stabilizing agents.

Trifluoroethanol is perhaps the most commonly used agent for stabilizing α-helix conformation in peptides (Moroder *et al.*, 1975; Lu *et al.*, 1984; Leist and Thomas, 1984; Dyson, *et al.*, 1988a, 1988b; Pena *et al.*, 1989; Lehrman *et al.*, 1990; Segawa, and Sugihara, 1984). Recently trifluoroethanol has been more thoroughly studied in this function (Sönnichsen, *et al.*, 1992; Jasanoff and Fersht, 1994). Sönnichsen *et al.* (1992) concluded that trifluoroethanol is not a helix-inducing solvent, *i.e.* it does not create new structures, but rather that it is a helix-enhancing cosolvent that stabilizes helices in regions with existing α-helical propensity. The dominant effect of trifluoroethanol is caused by its significantly weaker basicity with respect to that of water (Llinas and Klein, 1975), which decreases amide proton hydrogen bonding to the solvent and strengthens intramolecular hydrogen bonds, thereby stabilizing secondary structure (Nelson and Kallenbach, 1986).

For some time, this laboratory has been interested in a peptide derived from the C-terminal region of the fibrinogen γ-chain, residues 385–411 (Mayo *et al.* (1990) and references therein). During NMR and CD conformational studies of this 27-residue peptide (called γ27),[1] it was noticed that in the

* This work benefited from research grants from the W. W. Smith Charitable Trust and from the Pharmaceutical Research Institute, R. W. Johnson Co., Inc., Springhouse, PA. The costs of publication of this article were defrayed in part by the payment of page charges. This article must therefore be hereby marked "*advertisement*" in accordance with 18 U.S.C. Section 1734 solely to indicate this fact.

This paper is dedicated to the memory of Simon Pilkis, chair of the Biochemistry Department, who died suddenly August 2, 1995.

‡ To whom correspondence should be addressed: Dept. of Biochemistry, Biomedical Engineering Center, University of Minnesota, 420 Delaware St., S.E., Minneapolis, Minnesota 55455.

[1] The abbreviations used are: γ27, the 27-residue peptide derived from the C terminus of γ-chain fibrinogen, residues 385–411; NOE, nuclear Overhauser effect; NOESY, two-dimensional NMR nuclear Overhauser effect spectroscopy; HPLC, high pressure liquid chromatography; deg, degree(s).

presence or absence of trifluoroethanol, the average helix content determined by CD was increased on lowering the pH from 6 to 2. On the other hand, NOE magnitudes were decreased, suggesting the presence of either less structure or increased internal mobility at lower pH. The complications involved with interpreting NOEs from highly flexible, linear peptides arise from the fact that NOEs are sensitive to both the internuclear distance and internal motions. The present study was initiated to correlate pH-induced CD and NOE effects in γ27 with motional characteristics derived from $^{13}C_{\alpha}H$ relaxation experiments.

MATERIALS AND METHODS

Peptide Synthesis—A peptide representing amino acid residues 385–411 from human fibrinogen γ-chain (called γ27) was synthesized on a Milligen Biosearch 9600 automated peptide synthesizer. The procedures used were based on Merrifield solid phase synthesis utilizing Fmoc-BOP chemistry (Stewart and Young, 1984). After the sequence had been obtained, the peptide support and side chain protection groups were acid (trifluoroacetic acid and scavenger mixture)-cleaved. Crude peptides were analyzed for purity on a Hewlett-Packard 1090M analytical HPLC using a reverse phase C18 VyDac column. Peptides generally were about 90% pure. Further purification was done on a preparative reverse-phase HPLC C-18 column using an elution gradient of 0–60% acetonitrile with 0.1% trifluoroacetic acid in water. Peptides then were analyzed for amino acid composition on a Beckman 6300 amino acid analyzer by total hydrolysis (6 N HCl at 110 °C for 18–20 h) and by mass spectrometry. Final peptide purity was greater than 95%.

Circular Dichroism—Circular dichroism (CD) spectra were measured on a Jasco JA-710 air-cooled automatic recording spectropolarimeter coupled with a data processor. Curves were recorded digitally and fed through the data processor for signal averaging and base line subtraction. Spectra were recorded from 5 to 30 °C in 10 mM potassium phosphate, pH 2–6, over a 190–250-nm range using a 0.5-mm path length, thermally jacketed quartz cuvette. Temperature was controlled by using a Haacke water bath. Trifluoroethanol titrations were done up to 80% (v/v) trifluoroethanol. Peptide concentration was about 0.1 mM. The scan speed was 5.0 nm/min. Spectra were signal-averaged four times, and an equally signal-averaged solvent base line was subtracted. CD spectra were analyzed by the methods of Sreerama and Woody (1993) and Chen *et al.* (1974) for estimation of helix content.

NMR Measurements—Freeze-dried samples for NMR measurements were dissolved in either D_2O or H_2O/D_2O (9:1) containing 10 mM potassium phosphate. Protein concentration was in the range of 5 mM. pH was adjusted by adding microliter quantities of NaOD or DCl to the protein sample. For most experiments, the temperature was controlled at 5 °C. All NMR spectra were acquired on a Bruker AMX-600 NMR spectrometer.

For sequential assignments, two-dimensional NMR-correlated spectroscopy (Aue *et al.*, 1976; Wider *et al.*, 1984), double quantum-filtered two-dimensional NMR-correlated spectroscopy (Piantini *et al.*, 1982; Shaka and Freeman, 1983), and NOESY (Jeener *et al.*, 1979; Wider *et al.*, 1984) experiments were performed. Two-dimensional homonuclear magnetization transfer spectra, used to identify many spin systems completely, were obtained by spin locking with an MLEV-17 sequence (Bax and Davis, 1985) with a mixing time of 64 ms. All spectra were acquired in the phase-sensitive mode (States *et al.*, 1982). The water resonance was suppressed by direct irradiation (1 s) at the water frequency during the relaxation delay between scans as well as during the mixing time in NOESY experiments.

The majority of the two-dimensional NMR spectra were collected as 512 or 1024 t_1 experiments, each with 1024 or 2,048 complex data points over a spectral width of 5 kHz in both dimensions with the carrier placed on the water resonance. 64 or 96 scans were generally time-averaged per t_1 experiment. The data were processed directly on the Bruker AMX-600 X-32 or offline on a Bruker Aspect-1 work station using the UXNMR program. Data sets were multiplied in both dimensions by 0–60°-shifted sine-bell or lorentzian to gaussian transformation function and generally zero-filled to 1,024 in the t_1 dimension prior to Fourier transformation.

To obtain a quantitative description of peptide backbone dynamics, ^{1}H-detected ^{13}C heteronuclear chemical shift correlation spectra (van Mierlo *et al.* (1993) and references therein) were accumulated to derive (^{1}H)-^{13}C NOE and ^{13}C T_1 relaxation data on the unenriched peptide. In each case, cross-peak intensities depend on the relaxation parameter of interest. All spectra were acquired in the phase-sensitive mode by using time-proportional phase incrementation for quadrature detection in the ω_1 dimension; 2048 data points were recorded in each quadrature channel during t_2, and 200 real points were recorded in t_1. Spectra were acquired with a spectral width of 5000 Hz in ω_2 and 6000 Hz in ω_1. The ^{1}H carrier was placed on the HDO resonance, and the ^{13}C carrier was set at 45.4 ppm. For T_1 measurements, 128 scans were acquired per t_1 increment; for the NOE measurement, 256 scans were acquired per increment. For measurements of T_1 and NOE, a relaxation delay of 5.0 s was used between scans to ensure sufficient recovery of ^{1}H magnetization. For T_1 relaxation measurements, nine separate spectra were recorded for T = 0.01, 0.04, 0.08, 0.15, 0.2, 0.3, 0.6, 0.8, and 1.2 s. Relaxation rate constants and NOE enhancements were calculated from peak heights of the heteronuclear resonances as described by Palmer *et al.* (1991). Data analysis was performed on Bruker Aspect-1 or Silicon Graphics work stations using UXNMR, Aurelia (Bruker, Inc.), or FELIX (Biosym, Inc.) programs.

^{13}C NMR relaxation data were analyzed by using the model-free formalism of Lipari and Szabo (1982a, 1982b) in which motions are described in terms of two correlation times (an overall tumbling time and an internal motion correlation time) and an order parameter (S^2), which can be related to bond angular restrictions (Lipari and Szabo, 1982b). Since S^2 is least sensitive to τ_i, an average τ_i value of 5×10^{-11} s was used initially in the optimization routine and later varied up to 10×10^{-11} s. Then a resulting average τ_o value was fixed, and τ_i and S^2 were allowed to vary. In either case, S^2 varied by no more than 5%. Smaller values of the order parameter are taken to indicate relatively decreased motional restrictions.

Distance Geometry Calculations—The structures were calculated by using the constant valence force field included in the Biosym Software (INSIGHT II 2.3, DISCOVER 2.9) (San Diego, CA) on a Silicon Graphics Indigo 2. Distance constraints were derived from NOE data as discussed under "Results." Additional torsional restraints were applied to maintain trans-geometry and planarity for the peptide bond throughout the calculations. The starting extending polypeptide coordinate was minimized using 50 steps of steepest descent minimization and then 600 fs of molecular dynamics calculation at 1200 K with a step size of 1 fs followed by 500 steps of conjugate gradient minimization. After the triangle bounds smoothing was done, 30 coordinate files were created by metrization and embedding. Refinement of these coordinates was done using a simulated annealing protocol with a simplified error function to further optimize the fit between the coordinates and the distance matrix. The annealing protocol was followed by 1000 steps of conjugate gradient minimization to obtain the converged distance geometry-based structures.

RESULTS

Circular Dichroism—CD spectra of γ27 obtained at pH 6, 5 °C, are displayed in Fig. 1 at different trifluoroethanol concentrations. At 0% trifluoroethanol, the γ27 CD trace is characteristic of mostly random coil conformation. As the trifluoroethanol concentration is increased, the shape of the curves becomes increasingly characteristic of helical secondary structure. The monotonic trends in ellipticities and an apparent isodichroic point at about 204 nm suggest an equilibrium between two main conformational states, helix and random coil. Percentage of α-helicity was estimated by using the mean residue ellipticity at 220 nm [Θ_{220}] and the equation of Chen *et al.* (1974),

$$\Theta = (f_H - ik/N)\Theta_H \quad \text{(Eq. 1)}$$

where Θ is the observed mean residue ellipticity at 220-nm wavelength. Θ_H is the maximum mean residue ellipticity of a helix of infinite length (Chang *et al.*, 1978); f_H is the fraction of helix in the molecule; i is the number of helical segments; N is the total number of residues, and k is a wavelength-dependent constant (2.6 at 220 nm). The number of helical segments, i, was set to 2 in order to be consistent with modeled structures generated from NOE-derived distance constraints discussed later. The expected value of the mean residue ellipticity for 100% helicity of peptides of chain length 27 residues was determined to be −32,720 deg cm^2/dmol. Using this method, calculated helicities as a function of trifluoroethanol concentration are shown in the *inset* to

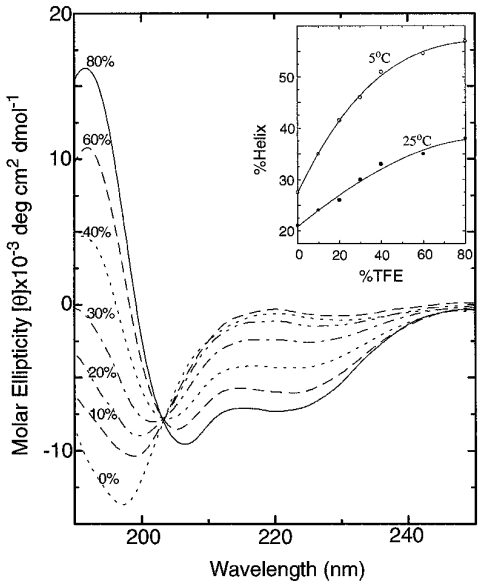

FIG. 1. **CD spectra of γ27.** CD spectra of γ27 obtained at pH 6 and 5 °C are shown at different trifluoroethanol concentrations as indicated in the *figure*. Trifluoroethanol concentrations are given as percentage (v/v) of composition. The peptide concentration was kept approximately constant at 40 μM. Based on CD data according to Equation 1, the calculated α-helix content in γ27 is plotted *versus* trifluoroethanol concentration in the *inset*. In the *inset*, data are shown for pH 6, 5 °C, and 25 °C. *Lines* drawn through *points* are for visual aid only.

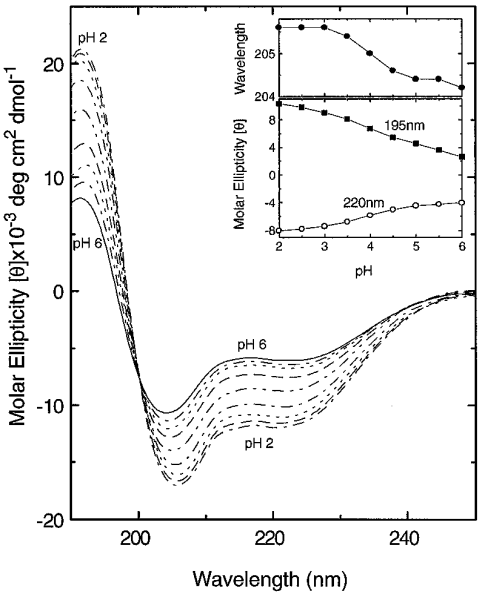

FIG. 2. **pH effect on CD spectra.** CD spectra for γ27 are plotted *versus* the solution pH from pH 2 to 6. In the *inset*, molar ellipticities are plotted for two wavelengths, 195 and 220 nm, as a function of the solution pH. At the *top* of the *inset*, wavelength in the 204–206-nm range is plotted *versus* the solution pH. trifluoroethanol concentration was constant at 40% (v/v). The temperature was 5 °C. Data points in the *inset* indicate the simple average of three pH titration series. Standard deviations are $\pm 0.5 \times 10^3$ deg cm^2 dmol^{-1} at 220 nm; $\pm 2 \times 10^3$ deg cm^2 dmol^{-1} at 195 nm; and ± 0.2 nm for the wavelength *versus* pH plot. *Lines* connecting *data points* are for visual aid only.

Fig. 1 for data accumulated at 5 and at 25 °C. As expected, helicity increased with increasing trifluoroethanol concentration and with decreasing temperature.

CD spectra are plotted as a function of solution pH (constant 40% trifluoroethanol and 5 °C) in Fig. 2. In the insert to Fig. 2, $[\Theta_{220}]$, $[\Theta_{195}]$, and the wavelength minimum in the 204–206-nm range, are plotted *versus* the solution pH. These

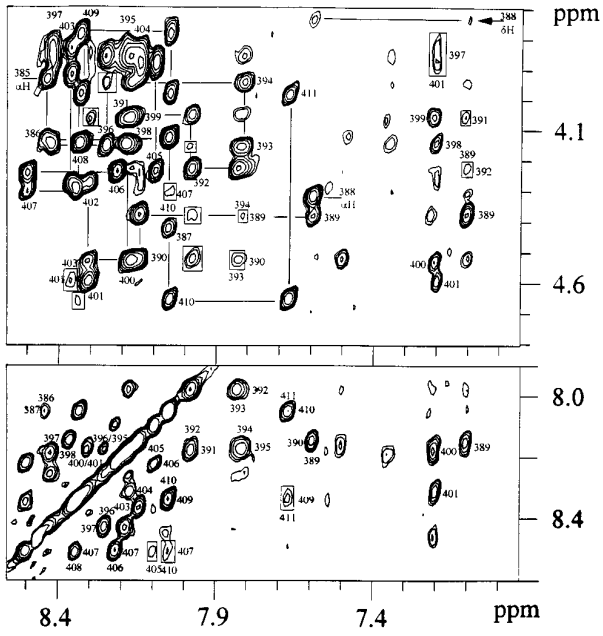

FIG. 3. **pH 5.3 NOESY contour plots of peptide γ27.** The αH-NH/aromatic and NH-NH/aromatic resonance regions from a NOESY contour plot are shown. Data were collected in 60% ^1H_2O/40% perdeuterated trifluoroethanol (0.6-ml total sample volume) with 10 mM peptide γ27 at pH 5.3 and 5 °C. 512 hypercomplex free induction decays containing 1024 words were collected and processed as discussed under "Materials and Methods." The mixing time was 0.1 s. The data were zero-filled to 1024 in t_1. The raw data were then multiplied by a 40°-shifted sine-squared function in t_1 and t_2 prior to Fourier transformation. Some sequential resonance assignments are traced out, and some longer range NOEs are indicated. Labeling of resonances is as discussed in the text.

CD data (*inset*) are consistent with increases in the average helix content of peptide γ27 as the pH is lowered from 6 to 2. Even though data shown in this figure have been accumulated in 40% trifluoroethanol, the same general trend is observed at lower trifluoroethanol concentrations. The isodichroic point at 200 nm supports the idea of an equilibrium between two main conformational populations, one having more helix character than the other.

NOEs and Distance Geometry Calculations—NOESY spectra of the αH-NH/aromatic and NH-NH/aromatic resonance regions of γ27 (5 °C and 40% trifluoroethanol) accumulated at pH 5.3 and at 2.5 are compared in Figs. 3 and 4, respectively. Since sequential resonance assignments for γ27 have been done at pH 3.5, 30 °C, 0% trifluoroethanol (Mayo *et al.*, 1990), they were easily made under the present solution conditions by using the standard approach outlined in Wüthrich (1986). Figs. 3 and 4 trace out some sequential assignments, which are tabulated more completely in Table I for pH 5.3 data. These data (Figs. 3 and 4) aim at identifying $d_{NN}(i, i + 1, 2)$, $d_{\alpha N}(i, i + n)$, and other relatively long range NOEs that help define conformational populations for γ27. These and other NOEs are summarized in Fig. 5 for pH values of 2.5 and 5.3. A complete listing of NOEs observed at pH 5.3 is given in Table II. Numerous $d_{NN}(i, i + n)$ and $d_{\alpha N}(i, i + n)$ NOEs are observed. At pH 5.3, most "longer range" NOEs are found within the sequence Phe^{389}–Glu^{396}. This network of NOEs suggests the presence of multiple-turn or helix-like structure. NOEs present at pH 5.3 normally are observed with similar or only slightly reduced magnitudes at pH 2.5. Cursory inspection of the NH-NH NOESY region may suggest large decreases in NOE magnitudes for data accumulated at pH 2.5. However, comparison with the αN region and normalization with Pro^{388}

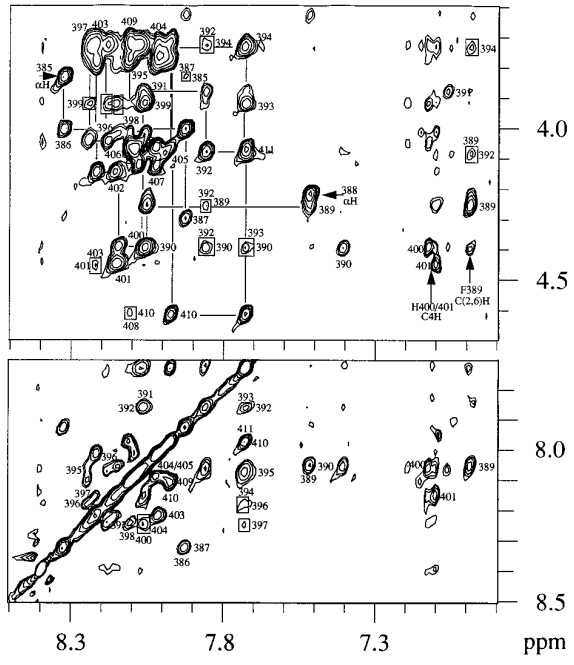

FIG. 4. **pH 2.5 NOESY contour plots of peptide γ27.** The αH-NH/aromatic and NH-NH/aromatic resonance regions from a NOESY contour plot are shown for data accumulated at pH 2.5. Data collection and processing was as discussed in the legend to Fig. 3 and in the text. Resonances are labeled as discussed in the text.

δH^1-δH^2 NOE indicates that NOE magnitudes are on average only slightly reduced. When comparing one segment with another, most NOEs that are reduced in intensity belong to residues within the C-terminal segment Gly^{403}–Val^{411}.

Distance constraints were derived from NOEs listed in Table II and were used in distance geometry calculations for conformational populations of γ27 at pH 5.3, 40% trifluoroethanol, 5 °C. The time dependence of NOEs was used to check for possible spin diffusion. Below about a 0.5-s mixing time in the NOESY experiment, spin diffusion could not be detected. NOEs were ranked relatively as strong (2.2–3 Å), medium (2.8–3.5 Å), and weak (3.3–5 Å). An additional 0.5 Å degree of freedom was allowed for each non-backbone atom (or pseudoatom) involved in any given distance constraint. Distance geometry calculations were first done by using XPLOR, followed by energy minimization and restrained annealing dynamics simulations. Electrostatic potentials for charged groups were varied from full charge to about 50% of full charge. 30 structures were generated. 10 of these showed minimal distance violations (from input NOE constraints) of less than 0.5 Å. Overall backbone RMSD values were less than 0.8 $Å^2$ for residues Phe^{389}–Glu^{396} and for residues Glu^{404}–Asp^{410}. Fig. 6 displays two sets of the same 10 structures generated this way. The *left portion* of the figure shows overlays for the N-terminal segment residues 389–396, and the *right portion* of the figure shows overlays for the C-terminal segment residues 404–410. Both N- and C-terminal segments form helix-like conformations. α-Helix character is greatest for sequences Arg^{391}–Gly^{395} and Ala^{405}–Gly^{409}. Ramachandran plots (data not shown) indicate that the greatest ψ,ϕ angular displacements are found for Gly^{397}–Gly^{403}. In this respect, it appears that the terminal segments move more or less as units connected via a mid-segment "hinge" region.

Electrostatic Interactions—pH-induced variances in CD ellipticities and NOE magnitudes indicate electrostatic modulation of γ27 conformational populations. Furthermore, chemical shift changes for most resonances are observed as a function of pH. The only titratable groups in γ27 belong to the carboxylate groups of Glu^{396}, Asp^{410}, and Val^{411}, and the side-chain imidazole groups of His^{400} and His^{401}. pK_a values (derived from plots of chemical shift *versus* pH) for Glu^{396}, Asp^{410}, and Val^{411} (data not shown) range from 3.7 to 4.1. For His^{401} and His^{400}, pK_a values of 6.5 and 6.6, respectively, can be estimated from the data shown in Fig. 7. Evidence for an electrostatic interaction between/among His^{400}, His^{401}, and Glu^{396} comes from the apparent Glu^{396} pK_a inflection observed in the titration curves of His^{400} and His^{401} C2 proton resonances. The lower pH portion of this titration curve (Fig. 7) has its chemical shift ordinate axis expanded in the *inset*. Data points have been connected with a *solid line*, which represents the sum of theoretical titration curves for Glu^{396} (pK_a of 4.1) and His^{400} (pK_a of 6.6). Proximity of His^{400} and Glu^{396} is confirmed by NOEs observed between His^{400}/His^{401} and Glu^{396}/Gly^{397} side-chain proton resonances (see Fig. 3 and Table II). Marqusee and Baldwin (1987) have observed that positive-negative side-chain electrostatic interactions are most stabilizing in a helical conformation when oppositely charged residues are at the i, $i + 4$ positions, respectively.

Significant pH-dependent chemical shift changes (greater than 0.1 ppm) for side chains of Lys^{385}, Ile^{386}, Arg^{391}, and Thr^{393} (data not shown) also argue for direct (although probably transient) interactions with Glu^{396}. In a helix-like conformation (Fig. 6), Thr^{393} is located at the i, $i + 3$ position with respect to Glu^{396}. Proximity to N-terminal residues Lys^{385} and Ile^{386} is considered plausible based on results from calculated structures. In particular, the side-chain of Lys^{385} can fold in toward the side-chain of Glu^{396} to mediate a "loose" electrostatic interaction. Within the Lys^{385}–His^{401} segment, 50% of these backbone NHs are shifted more than 0.1 ppm on varying the pH between 2.5 and 5.3. In particular, two of the more shifted NHs belong to Ile^{387} and Phe^{389}, supporting the idea of a possible long range structurally stabilizing effect of Glu^{396}. Additionally, Ile^{387} NH is one of the most long lived NHs at lower pH (Mayo *et al.*, 1990). This electrostatic interaction in combination with hydrophobic side-chain clustering (Dyson *et al.*, 1992), could explain this NH solvent protection.

Protonation/deprotonation of Asp^{410} and Val^{411} (C-terminal carboxylate) probably plays no role in the electrostatic effects of the N-terminal and mid-peptide segments. The only side chain within C-terminal residues Leu^{402}–Val^{411} that shows significant chemical shifts on varying pH belongs to Ala^{405}. Other residues have their backbone resonances more highly shifted than their side-chain resonances, suggestive of indirect, conformationally induced chemical shift changes. In particular, the noncharged amino acid residue NHs of Gln^{407}, Ala^{408}, and Gly^{409} are shifted by between 0.15 and 0.25 ppm, and Gly^{409} αHs are more degenerate at lower pH. Interestingly, side-chain proton resonances of Lys^{406} demonstrate a carboxylate pK_a inflection. This suggests an electrostatic interaction between Lys^{406} and most probably Asp^{410} or Val^{411}.

γ27 Backbone Dynamics—^{1}H-detected two-dimensional heteronuclear ^{13}C NMR experiments (Nirmala and Wagner, 1988; Kay *et al.*, 1989; Clore *et al.*, 1990; Palmer *et al.*, 1991) have been used to characterize $^{13}C_\alpha$ relaxation in γ27, thereby providing information on local peptide backbone motional restrictions. $^{13}C_\alpha$ resonance assignments were made by correlating $^1H_\alpha$ resonances to the corresponding $^{13}C_\alpha$ resonances in ^{1}H-detected ^{13}C heteronuclear shift correlation experiments (van Mierlo *et al.*, 1993) done at pH values between 2.5 and 5.3. $^{13}C_\alpha$ chemical shifts at pH 5.3 are listed in Table I. Typical $(^1H)^{-13}C$ NOE data are shown in Fig. 8, and $^{13}C_\alpha$ T_1 and (^1H)-$^{13}C_\alpha$ NOE data accumulated at pH 2.5 and pH 5.3 are compared in Fig. 9. Relaxation data for glycines were not derived due to resonance

TABLE I

^1H- and $^{13}C_\alpha$ NMR sequence-specific resonance assignments (ppm)

Solution conditions are pH 5.3, 278 K, 40% trifluoroethanol, 60% ^1H_2O. The HDO resonance is 4.86 ppm downfield from TSP.

Residue	NH	αH	βH	Others	$^{13}C_\alpha$
Lys^{385}		3.95	1.82	γH$_2$ 1.36 δH$_2$ 1.64 εH$_2$ 2.91	51.36
Ile^{386}	8.45	8.14	1.72	γH$_3$ 1.09 γH$_2$ 1.43 δH$_3$ 0.77	56.9
Ile^{387}	8.06	4.43	1.76	γH$_3$ 1.07 γH$_2$ 1.43 δH$_3$ 0.75	59.06
Pro^{388}		4.33	2.06, 2.06	γH$_2$ 1.86 δH$_2$ 3.51, 3.75	53.85
Phe^{389}	7.60	4.39	3.03, 2.94		54.3
Asn^{390}	8.16	4.54	2.81, 2.81		49.25
Arg^{391}	8.18	4.06	1.84, 1.77	γH$_2$ 1.60 δH$_2$ 3.11	53.05
Leu^{392}	7.99	4.24	1.72, 1.56		51.86
Thr^{393}	7.84	4.23	4.17	γH$_3$ 1.13	58.62
Ile^{394}	7.82	3.96	2.04	δH$_3$ 0.84 γH$_3$ 1.08 γH$_2$ 1.43	58.54
Gly^{395}	8.19	3.87, 3.87			
Glu^{396}	8.26	4.16	2.02	γH$_2$ 2.32, 2.28	53.08
Gly^{397}	8.44	3.83, 3.88			
Gln^{398}	8.20	4.16	2.06, 2.02	γH$_2$ 2.35, 2.29	52.91
Gln^{399}	8.21	4.08	1.96, 1.91	γH$_2$ 2.30, 2.34	52.66
His^{400}	8.18	4.55	3.21, 3.07		51.53
His^{401}	8.32	4.61	3.25, 3.15		51.53
Leu^{402}	8.32	4.29	1.63, 1.53	γH 1.53 δH$_3$ 0.77	51.14
Gly^{403}	8.37	3.36, 3.93			
Gly^{404}	8.16	3.89			
Ala^{405}	8.10	4.24	1.32		48.37
Lys^{406}	8.23	4.25	1.79, 1.71	γH$_2$ 1.41, 1.37 δH$_2$ 1.61 εH$_2$ 2.91	49.14
Gln^{407}	8.51	4.31	2.09, 1.92	γH$_2$ 2.31	52.14
Ala^{408}	8.35	4.16	1.34		49.14
Gly^{409}	8.34	3.80,3.99			
Asp^{410}	8.06	4.66	2.74, 2.65		50.03
Val^{411}	7.68	4.00	2.04	γH$_3$ 0.84	59.31

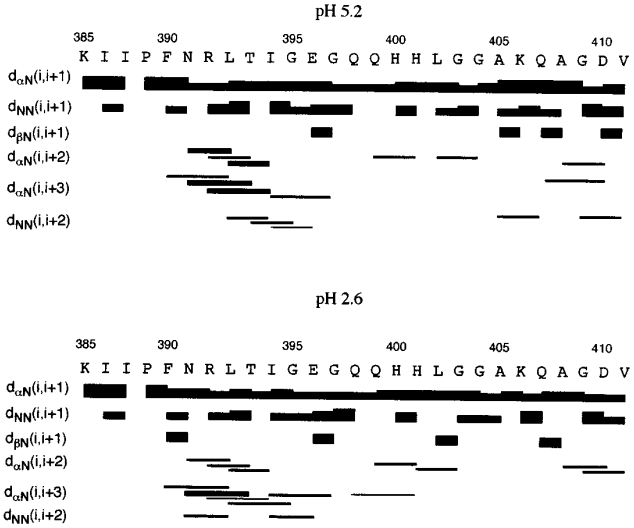

FIG. 5. **Summary of NOE data for peptide γ27.** The peptide sequence of γ27 is shown with a summary of identifiable NOEs given *above* for data accumulated at pH 5.3 and *below* for data accumulated at pH 2.5. NOEs are tabulated in the format discussed by Wüthrich (1986). A *question mark* indicates ambiguity in identifying a possible NOE.

overlap of the five glycines. Furthermore, due to spectral overlap of some other ^1H-^{13}C cross-peaks, *i.e.* Leu^{392} with Leu^{402} and Gln^{407}, and Glu^{396} with Gln^{398}, relaxation parameters for these cross-peaks could not be as accurately determined as those for others. T_1 relaxation curves, however, did appear linear; therefore, individual respective relaxation rates are similar for these partially overlapped cross-peaks.

Within the N-terminal segment Lys^{385}–Phe^{389}, both T_1 and NOE values are smaller for γ27 at pH 5.3, indicating decreased backbone mobility of that sequence at higher pH. This is reflected in order parameters, S^2, derived from these relaxation data (Fig. 9). For residues Ala^{405}–Val^{411}, S^2 values are larger at pH 2.5, indicating increased motional restriction of the C-terminal segment at lower pH. For residues Asn^{390}–His^{401}, S^2 values vary less with pH change. At either pH, the mid-peptide region residues Thr^{393}–His^{400} generally show the smallest order parameters, indicating the presence of a relatively flexible mid-peptide segment, consistent with NOE-based distance geometry calculations, which indicate an ill-defined mid-peptide segment from about Gly^{395} to His^{401}. The overall correlation time, τ_o, was 1.9 ns at either pH value.

DISCUSSION

Short, linear peptides, like γ27, generally exist in solution in an ensemble of highly fluctuating structures whose NMR spectral parameters average. This is true for γ27 in aqueous solution at 30 °C in the absence of trifluoroethanol (Mayo *et al.*, 1990) where multiple turn or nascent helix (Dyson *et al.*, 1988a, 1988b) conformation was apparent within residues 385–402. Under those solution conditions, C-terminal residues 402–411 showed no NOE structural constraints greater than i, $i + 1$; however, conformational preference within that segment was

TABLE II
^{1}H NMR-derived distance constraints used in computer modeling

NOE				Intensity[a]
From		To		
Lys^{385}	αH	Ile^{386}	NH	s
Ile^{386}	αH	Ile^{387}	NH	s
	NH	Ile^{387}	NH	w
	αH	Lys^{385}	βH	vw
	NH	Lys^{385}	γH	m
Ile^{387}	NH	Pro^{388}	δH	vw
	αH	Pro^{388}	δH	s
	NH	Ile^{386}	γH	m
Pro^{388}	αH	Phe^{389}	NH	s
	αH	Phe^{389}	2,6H	w
Phe^{389}	αH	Asn^{390}	NH	s
	αH	Leu^{392}	NH	vw
	NH	Asn^{390}	NH	s
	NH	Pro^{388}	δH	vw
	2,6H	Pro^{388}	δH	vw
	NH	Asn^{390}	γH	s
	NH	Pro^{388}	γH	m
	NH	Ile^{387}	δH	s
	2,6H	Leu^{392}	αH	vw
	2,6H	Asn^{390}	γH	vw
	2,6H	Pro^{388}	γH	w
	2,6H	Thr^{393}	γH	w
	2,6H	Ile^{387}	δCH_3	w
	2,6H	Leu^{392}	δCH_3	w
	2,6H	Ile^{387}	γH	vw
	2,6	Leu^{392}	γH	vw
	2,6H	Asn^{390}	αH	w
	γH	Pro^{388}	γH	vw
	NH	Pro^{388}	γH	m
	NH	Ile^{387}	δCH_3	m
	NH	Ile^{387}	δCH_3	vw
	αH	Arg^{391}	γH	vw
	αH	Leu^{392}	γH	w
	αH	Leu^{392}	γH	w
	αH	Thr^{393}	γH	vw
Asn^{390}	αH	Arg^{391}	NH	ms
	αH	Leu^{392}	NH	w
	αH	Thr^{393}	γH	vw
	αH	Thr^{393}	NH	vw
	αH	Phe^{389}	NH	vw
	αH	Phe^{389}	2,6H	w
	NH	Phe^{389}	NH	s
	NH	Phe^{389}	2,6H	m
	NH	Phe^{389}	γH	m
	γNH2	Thr^{393}	γH	w
	αH	Arg^{391}	γH	vw
	αH	Arg^{391}	γH	vw
	NH	Arg^{391}	γH	vw
	NH	Arg^{391}	γH	vw
	γNH2	Arg^{391}	γH	vw
	γNH2	Ile^{386}	δH	vw
	γNH2	Ile^{386}	γH	vw
	γNH2	Ile^{394}	δH	vw
	γNH2	Arg^{391}	NH	vw
Arg^{391}	αH	Leu^{392}	NH	ms
	αH	Thr^{393}	NH	w
	αH	Ile^{394}	NH	w
	NH	Leu^{392}	NH	s
	αH	Asn^{390}	γH	w
	αH	Ile^{394}	δCH_3	vw
	αH	Ile^{394}	γCH_3	vw
	αH	Ile^{394}	δH	w
Leu^{392}	αH	Thr^{393}	NH	s
	NH	Arg^{391}	NH	s
	NH	Arg^{391}	δCH_2	vw
	NH	Asn^{390}	γH	w
	NH	Thr^{393}	γH	vw
	NH	Arg^{391}	γH	w
	NH	Arg^{391}	γH	w
	αH	Asn^{390}	γH	vw
Thr^{393}	αH	Ile^{394}	NH	ms
	NH	Leu^{392}	NH	s
	NH	Asn^{390}	γH	vw
	NH	Glu^{396}	γH	vw
	NH	Leu^{392}	δH	vw
	NH	Leu^{392}	γH	w

TABLE II—*continued*
^{1}H NMR-derived distance constraints used in computer modeling

NOE				Intensity[a]
From		To		
	αH	Leu^{392}	γH	vw
	αH	Glu^{396}	γH	vw
Ile^{394}	αH	Gly^{395}	NH	s
	αH	Glu^{396}	NH	vw
	NH	Glu^{396}	γH	vw
	NH	Glu^{396}	γH	vw
	αH	Glu^{396}	γH	vw
Gly^{395}	αH	Glu^{396}	NH	s
	αH	Ile^{394}	NH	vw
	NH	Ile^{394}	NH	s
	NH	Thr^{393}	NH	w
	αH	Glu^{396}	γH	w
	αH	Glu^{396}	γH	w
	αH	Ile^{394}	γH	w
	αH	Ile^{394}	δH	w
Glu^{396}	αH	Gly^{397}	NH	s
	NH	Gly^{395}	NH	m
	NH	Thy^{393}	γH	vw
	NH	Ile^{394}	δH	vw
	αH	Gln^{399}	γH	w
Gly^{397}	αH	Gln^{398}	NH	m
	αH	His^{400}	4H	w
	NH	Glu^{396}	NH	s
	NH	Glu^{396}	γH	m
	NH	Glu^{396}	γH	w
Gln^{398}	αH	Gln^{399}	NH	m
	αH	His^{401}	4H	w
	NH	Gly^{397}	NH	s
Gln^{399}	NH2	His^{400}	NH	vw
	αH	His^{400}	NH	ms
	αH	His^{400}	4H	m
	αH	Leu^{402}	δH	vw
	αH	Gln^{398}	γH	vw
His^{400}	αH	His^{401}	NH	ms
	4H	Gln^{398}	αH	m
	4H	Gly^{397}	αH	w
	4H	Glu^{396}	αH	w
	4H	Glu^{396}	γH	vw
	4H	Glu^{396}	γH	vw
	4H	Gln^{399}	γH	vw
	4H	Gln^{399}	γH	vw
His^{401}	αH	Leu^{402}	NH	m
	αH	Gly^{403}	NH	vw
	NH	His^{400}	NH	s
	NH	His^{400}	γH	m
	NH	Gln^{399}	γH	vw
	NH	Gln^{399}	γH	vw
	NH	Gln^{398}	γH	vw
	4H	Leu^{402}	αH	vw
	NH	Gln^{398}	γH	vw
	NH	Leu^{402}	γH	vw
	NH	Leu^{402}	δH	vw
	αH	Leu^{402}	γH	vw
	αH	Leu^{402}	γH	vw
Leu^{402}	αH	Gly^{403}	NH	s
	NH	Gln^{399}	αH	w
	αH	Ala^{405}	γH	vw
Gly^{403}	αH	Gly^{404}	NH	s
	NH	Leu^{402}	γH	m
	NH	Leu^{402}	δH	m
	αH	Ala^{405}	γH	vw
Gly^{404}	αH	Ala^{405}	NH	s
	NH	Gly^{403}	NH	s
	NH	Ala^{405}	γH	vw
	αH	Ala^{405}	γH	w
	αH	Glu^{407}	γH	vw
Ala^{405}	αH	Lys^{406}	NH	s
	αH	Ala^{408}	γH	vw
	αH	Gln^{407}	γH	vw
	αH	Gln^{407}	γH	w
Lys^{406}	αH	Gln^{407}	NH	s
	NH	Ala^{405}	NH	m
	NH	Ala^{405}	γH	s
	αH	Asp^{410}	γH	vw
Gln^{407}	αH	Ala^{408}	NH	s
	αH	Asp^{410}	NH	vw

TABLE II—*continued*
^{1}H NMR-derived distance constraints used in computer modeling

NOE				Intensity[a]
From		To		
	NH	Lys^{406}	NH	s
	NH	Asp^{410}	γH	w
	NH	Lys^{406}	γH	m
	NH	Lys^{406}	δH	vw
	NH	Ala^{408}	γH	vw
	NH2	Ala^{408}	γH	vw
	αH	Ala^{408}	γH	vw
Ala^{408}	αH	Gly^{409}	NH	s
	αH	Asp^{410}	NH	w
	NH	Asp^{410}	γH	vw
	NH	Gln^{407}	γH	s
	NH	Gln^{407}	γH	s
	αH	Val^{411}	γH	w
Gly^{409}	αH	Asp^{410}	NH	s
	NH	Gln^{407}	γH	m
	NH	Gln^{407}	γH	m
Asp^{410}	αH	Val^{411}	NH	s
	αH	Gly^{409}	NH	vw
	NH	Gly^{409}	NH	s
	NH	Gln^{407}	NH	vw
	NH	Gln^{407}	γH	vw
	NH	Gln^{407}	γH	vw
	NH	Ala^{408}	γH	w
	αH	Val^{411}	γH	vw
Val^{411}	NH	Asp^{410}	NH	s
	NH	Gly^{409}	NH	vw
	NH	Asp^{410}	γH	ms
	NH	Ala^{408}	γH	vw
	αH	Asp^{410}	γH	vw
	αH	Lys^{406}	εH	vw
	αH	Ala^{408}	γH	vw

[a] Relative NOE intensities have been derived by volume integration and/or contour level counting and are classified as strong (s), medium (m), weak (w), and very weak (vw) with the following assigned distance bounds: strong NOEs, 1.8–2.8 Å; medium NOEs, 1.8–3.3 Å; weak NOEs, 1.8–4.0 Å, and very weak NOEs, 1.8–5.0 Å. For NOEs to side-chain groups, 0.5 Å was added to the upper distance.

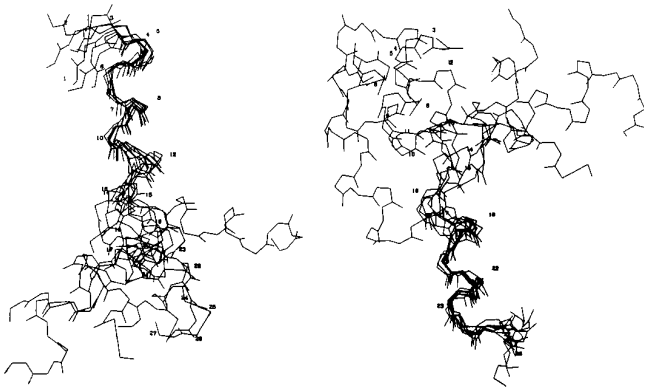

FIG. 6. **Computer-modeled structures of γ27.** Based primarily on NOE-derived distance constraints, distance geometry, restrained minimization, and dynamics, simulated annealing calculations were performed using the XPLOR program on an SGI 480 computer. The superposition of backbone atoms of 10 structures are shown as discussed in the text. On the *left side* of the *figure*, the best overlay for N-terminal residues is shown, while on the *right side*, the best overlay for C-terminal residues is shown. In this *figure*, residues are labeled from 1 to 27 instead of from 385 to 411.

apparent based on chemical shift differences with fibrinogen γ-chain peptide 400–411 and a 5-Hz $^3J_{\alpha N}$ coupling constant for Ala^{408} (Mayo *et al.*, 1990). This observation is supported with NMR studies on fibrinogen γ-chain peptide 392–411 done by Blumenstein *et al.* (1992), who reported that at 5 °C (also in the absence of trifluoroethanol), a significant β-turn population exists for the sequence Gln^{407}–Asp^{410}.

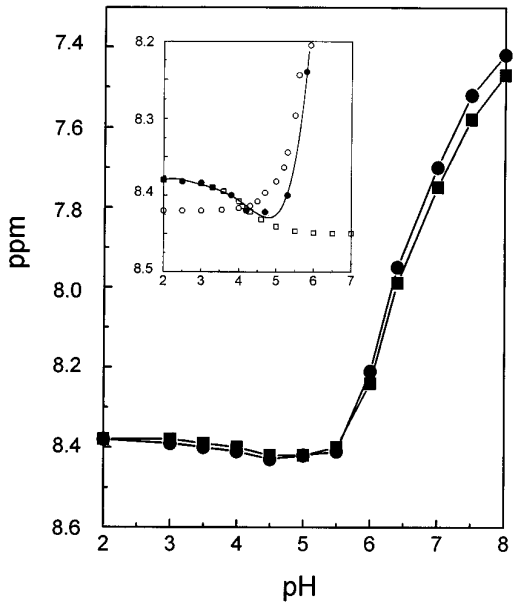

FIG. 7. **Chemical shift *versus* pH for His^{400} and His^{401} C2.** Chemical shifts for His^{400} and His^{401} C2 proton resonances are plotted *versus* the solution pH. The insert expands the chemical shift *ordinate axis* to better display the lower pH inflection in the histidine titrations curves. Data for His^{400} alone are shown connected by the *solid line*. *Solid* and *open squares* indicate calculated titration curves for Glu^{396} with a pK_a of 4.1 and for His^{400} with a pK_a of 6.6. These two theoretical curves sum up to yield the *solid line* drawn through the His^{400} data points.

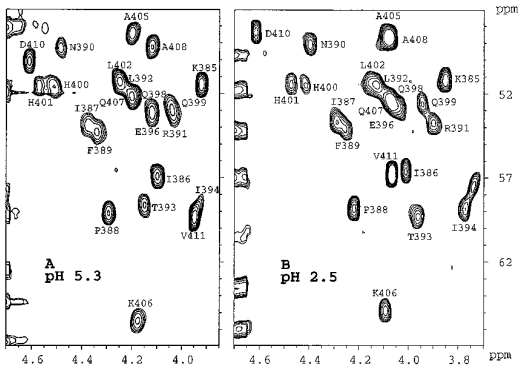

FIG. 8. **(^{1}H)-^{13}C Hetcor NOE Data.** Two ^{1}H-^{13}C heteronuclear shift-correlated NOE data sets (van Mierlo *et al.*, 1993) are shown for γ27 at pH 5.3 (*A*) and pH 2.5 (*B*). Resonances have been assigned as discussed in the text.

These present γ27 NOE data accumulated in the presence of trifluoroethanol are consistent with both reports (Mayo *et al.*, 1990; Blumenstein *et al.*, 1992). More transient multiple turn or helix-like conformations noted at 30 or 5 °C in the absence of trifluoroethanol are stabilized by the presence of trifluoroethanol, which acts as a structure-enhancing cosolvent (Sönnichsen, *et al.*, 1992; Jasanoff and Fersht, 1994), rather than as a conformation-inducing, *i.e.* new structure-inducing, agent. Trifluoroethanol stabilizes helix conformation in peptide sequences that have some helix propensity. The Chou-Fasman (1978) predictive secondary structure algorithm yields good probabilities for helix formation from residues Leu^{392}–Leu^{402} as well as from residues Ala^{405}–Val^{411} (Mayo *et al.*, 1990). At pH 5.3, NOE-based distance geometry-generated structures of γ27 indicate that helix-like or multiple turn conformations are present within the N- and C-terminal segments, residues 391–397 and 404–408, respectively. N-terminal residues 385–387 have an extended conformation, and Pro^{388} causes a kink in the

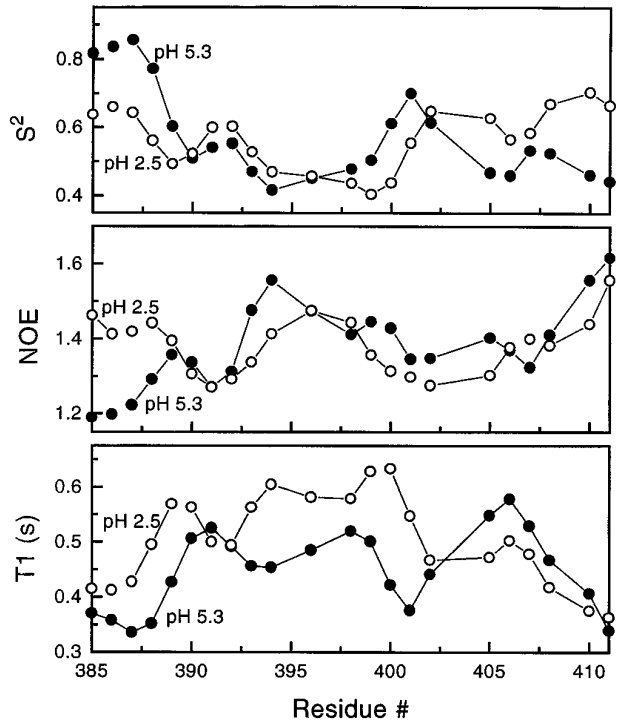

FIG. 9. **γ27 ^{13}C T_1, NOE, and order parameters.** ^{13}C T_1, (^{1}H)-^{13}C NOE data, and backbone motional order parameters, S^2, for γ27 at pH 2.5 and at pH 5.3 are shown. As discussed under "Materials and Methods" and in the text, order parameters, S^2, have been derived from these relaxation data by using the model-free approach of Lipari and Szabo (1982a, 1982b).

structure that leads into a turn centered at 390–391. The trifluoroethanol-stabilized, N-terminal conformation, residues 385–397, is essentially the same as that observed for γ27 in aqueous solution at 30 °C (Mayo *et al.*, 1990), once again supporting the idea that trifluoroethanol does not induce new structure formation but rather acts to enhance existing conformational populations (Söennichsen *et al.*, 1992; Jasanoff and Fersht, 1994). Within the Gly^{397}–Gly^{403} segment, few "long range" NOEs are observed, which results in distance geometry calculations of a conformationally ill defined mid-peptide region. The paucity of NOEs could be the result of a more extended, solvent-exposed conformation and/or of a more flexible domain. Since average motional order parameters are reduced within this region relative to other sequences, one can conclude that the mid-peptide segment is relatively more flexible than any other segment. The lack of conformationally constraining NOEs within this region, therefore, is mostly due to the presence of an ensemble of highly fluctuating conformations. In this respect, N- and C-terminal helix-like regions are connected by a "hinge" segment. In support of this, it should be noted that glycine, which highly populates this mid-peptide segment (Gly^{395}, Gly^{397}, Gly^{403}, Gly^{404}), normally promotes increased ψ,ϕ angular freedom and flexibility, disrupts periodic structure, and frequently occupies the helix C-cap position (Richardson and Richardson, 1988).

In terms of the effect of pH on specific sequences within γ27, NMR data indicate that N- and C-terminal domains behave differently. Generally, the same NOEs are observed at either pH 2.5 or pH 5.3, indicating the presence of similar conformational populations. NOE magnitudes at pH 2.5, however, are reduced on average by about 10–20% relative to those observed at pH 5.3. Most NOE magnitudes observed within the mid-peptide region are unaffected by pH changes. Within the N-terminal segment, which becomes more flexible at lower pH, however, NOE magnitudes are generally reduced, suggesting a more "open" or less structured γ27 N-terminal conformation at pH 2.5. This is consistent with results from protein folding studies where decreasing the pH to 2–3 denatures or unfolds protein structures. Consistent with distance geometry structural calculations, Lys^{385} and the N-terminal amine may interact electrostatically with Glu^{396}; and by neutralizing Glu^{396} by lowering pH these charge-charge interactions are minimized or negated, causing the N-terminal segment to become less conformationally and dynamically restricted, resulting in reduced NOE magnitudes.

Unlike the N-terminal domain, the C-terminal segment, residues Ala^{405}-Val^{411}, becomes more motionally restricted at lower pH. In apparent contradiction to this, NOE magnitudes, particularly those of NH-NH, are reduced for these C-terminal residues, while the change in CD molar ellipticity translates into an approximately 15% increase in average helix content. For short linear peptides that exist in a highly dynamic conformational ensemble that displays some average "structure," NOEs are difficult to interpret since they are affected both by changes in internuclear distances and by motional properties of the peptide. Increased negative CD ellipticities at 224 nm could be the result of increased β-turn character at the higher pH value, which would show a more positive absorption at 224 nm and would reduce the apparent negative ellipticity at 220 nm (Dyson *et al.*, 1988a and 1988b). In this respect, these results suggest that the γ27 conformational ensemble is shifted to a more helical character at lower pH. Reduced NH-NH NOE magnitudes, for example, would be explained by increased average NH-NH internuclear distances in a helical conformation relative to a tight turn.

In conclusion, this study has shown that for the more hydrophobic N-terminal segment that may be partially stabilized by electrostatic interactions, lowering the pH induces a more open, more dynamic conformational ensemble, while for the C-terminal segment lowering the pH shifts this ensemble to a more helical, less flexible conformational distribution. For γ27, pH has the effect of acting at the local, rather than global, conformational level.

Acknowledgments— NMR experiments were performed at the University of Minnesota High Field-NMR Laboratory. Peptides were synthesized at the Microchemical Facility, Institute of Human Genetics, University of Minnesota. We are very grateful to Dinesha S. Walek and Marek Kloczewiak for expertise in peptide synthesis and to Vladimir Daragan and Vikram Roongta for helpful discussions on ^{13}C relaxation studies.

REFERENCES

Aue, W. P., Bartholdi, E. & Ernst, R. R. (1976) *J. Chem. Phys.* **64,** 2229–2246
Bax, A. & Davis, D. G. (1985) *J. Magn. Reson.* **65,** 355–360
Blumenstein, M., Matsueda, G. R., Timmons, S. & Hawiger, J. (1992) *Biochemistry* **31,** 10692–10698
Brown, J. E. & Klee, W. A. (1971) *Biochemistry* **10,** 470–476
Chang, C. T., Wu, C. S. C. & Yang, J. T. (1978) *Anal. Biochem.* **91,** 13–31
Chen, Y. H., Yang, J. T. & Chau, K. H. (1974) *Biochemistry* **13,** 3350–3359
Chou, P. Y. & Fasman, G. D. (1978) *Adv. Enzymol. Relat. Areas Mol. Biol.* **48,** 45–148
Clore, G. M., Driscoll, P. C., Wingfield, P. T. & Gronenborn, A. M. (1990) *Biochemistry* **29,** 7387–7401
Conio, G., Patrone, E. & Brighetti, S. (1970) *J. Biol. Chem.* **245,** 3335–3340
Dyson, H. J., Sayre, J. R., Merutka, G., Shin, H.-C., Lerner, R. A. & Wright, P. E. (1992) *J. Mol. Biol.* **226,** 819–835
Dyson, H. J., Rance, M., Houghten, R. A., Lerner, R. A. & Wright, P. E. (1988a) *J. Mol. Biol.* **201,** 161–200
Dyson, H. J., Rance, M., Houghten, R. A., Wright, P. E. & Lerner, R. A. (1988b) *J. Mol. Biol.* **201,** 201–217
Goto, Y., Calciano, L. & Fink, A. (1990) *Proc. Natl. Acad. Sci. U. S. A.* **87,** 573–577
Ilyina, E., Milius, R. & Mayo, K. H. (1994) *Biochemistry* **33,** 13436–13444
Jaenicke, R. (1991) *Biochemistry* **30,** 3147–3161
Jasanoff, A. & Fersht, A. R. (1994) *Biochemistry* **33,** 2129–2135
Jeener, J., Meier, B. H., Bachman, P. & Ernst, R. R. (1979) *J. Chem. Phys.* **71,** 4546–4553
Kay, L. E., Torchia, D. A. & Bax, A. (1989) *Biochemistry* **28,** 8972–8979
Kuwajima, K. (1992) *Curr. Opin. Biotechnol.* **3,** 462–467
Lehrman, S. R., Tuls, J. L. & Lund, M. (1990) *Biochemistry* **29,** 5590–5596

Leist, T. & Thomas, R. M. (1984) *Biochemistry* **23,** 2541–2547
Lipari, G. & Szabo, A. (1982a) *J. Am. Chem. Soc.* **104,** 4546–4559
Lipari, G. & Szabo, A. (1982b) *J. Am. Chem. Soc.* **104,** 4559–4570
Llinas, M. & Klein, M. P. (1975) *J. Am. Chem. Soc.* **97,** 4731–4737
Lu, Z. X., Fok, K. F., Erickson, B. W. & Hugli, T. E. (1984) *J. Biol. Chem.* **259,** 7367–7370
Marqusee, S. & Baldwin, R. L. (1987) *Proc. Natl. Acad. Sci. U. S. A.* **84,** 8898–8902
Mayo, K. H., Burke, C., Lindon, J. N. & Kloczewiak, M. (1990) *Biochemistry* **29,** 3277–3286
Moroder, L., Filippi, B., Borin, G. & Marchiori, F. (1975) *Biopolymers* **14,** 2075–2093
Nelson, J. W. & Kallenbach, N. R. (1986) *Proteins* **1,** 211–217
Nirmala, N. R. & Wagner, G., (1988) *J. Am. Chem. Soc.* **110,** 7557–7558
Palmer, A. G., III, Rance, M. & Wright, P. E. (1991) *J. Am. Chem. Soc.* **13,** 4371–4380
Parodi, R. M., Bianchi, E., and Ciferri, A. (1973) *J. Biol. Chem.* **248,** 4047–4051
Pena, M. C., Rico, M., Jimenez, M. A., Herranz, J., Santoro, J. & Nieto, J. L. (1989) *Biochim. Biophys. Acta* **957,** 380–389
Piantini, U., Sørensen, O. W. & Ernst, R. R. (1982) *J. Am. Chem. Soc.* **104,** 6800–6805
Richardson, J. S. & Richardson, D. C. (1988) *Science* **240,** 1648–1652
Sanz, J. M., Johnson, C. M. & Fersht, A. R. (1994) *Biochemistry* **33,** 11189–11199
Savage, B. & Ruggeri, Z. M. (1991) *J. Biol. Chem.* **266,** 11227–11233
Segawa, S.-I. & Sugihara, M. (1984) *Biopolymers* **23,** 2473–2488
Shaka, A. J. & Freeman, R. (1983) *J. Magn. Reson.* **51,** 161–169
Shin, H. C., Merutka, G., Waltho, J. P., Wright, P. E. & Dyson, H. J. (1993a) *Biochemistry* **32,** 6348–6355
Shin, H. C., Merutka, G., Waltho, J. P., Tennant, L. L., Dyson, H. J. & Wright, P. E. (1993b) *Biochemistry* **32,** 6356–6364
Sönnichsen, F. D., Van Eyk, J. E., Hodges, R. S. & Sykes, B. D. (1992) *Biochemistry* **31,** 8790–8798
Sreerama, N. & Woody, R. W. (1993) *Anal. Biochem.* **209,** 32–44
Stewart, J. M. & Young, J. D. (1984) *Solid Phase Peptide Synthesis*, 2nd Ed., Pierce Chemical Co., Rockford, IL
States, D. J., Haberkorn, R. A., and Ruben, D. J. (1982) *J. Magn. Reson.* **48,** 286–293
van Mierlo, C. P. M., Darby, N. J., Keeler, J., Neuhaus, D. & Creighton, T. E. (1993) *J. Mol. Biol.* **229,** 1125–1146
Waltho, J. P., Feher, V. A., Merutka, G., Dyson, H. J. & Wright, P. E. (1993) *Biochemistry* **32,** 6337–6347
Wider, G., Macura, S., Anil-Kumar, Ernst, R. R. & Wüthrich, K. (1984) *J. Magn. Reson.* **56,** 207–234
Wüthrich, K. (1986) *NMR of Proteins and Nucleic Acids*, Wiley-Interscience, New York
Yang, Y., Barker, S., Chen, M.-J. & Mayo, K. H. (1993) *J. Biol. Chem.* **268,** 9223–9229